Monolayers of Silver Nanoparticles Decrease Photobleaching: Application to Muscle Myofibrils

P. Muthu,* N. Calander,* I. Gryczynski,† Z. Gryczynski,* J. M. Talent,* T. Shtoyko,‡ I. Akopova,* and J. Borejdo*
*Department of Molecular Biology and Immunology, and †Department of Cell Biology and Genetics, University of North Texas Health Science Center, Fort Worth, Texas; and ‡Department of Chemistry, University of Texas at Tyler, Tyler, Texas

ABSTRACT Studying single molecules in a cell has the essential advantage that kinetic information is not averaged out. However, since fluorescence is faint, such studies require that the sample be illuminated with the intense light beam. This causes photodamage of labeled proteins and rapid photobleaching of the fluorophores. Here, we show that a substantial reduction of these types of photodamage can be achieved by imaging samples on coverslips coated with monolayers of silver nanoparticles. The mechanism responsible for this effect is the interaction of localized surface plasmon polaritons excited in the metallic nanoparticles with the transition dipoles of fluorophores of a sample. This leads to a significant enhancement of fluorescence and a decrease of fluorescence lifetime of a fluorophore. Enhancement of fluorescence leads to the reduction of photodamage, because the sample can be illuminated with a dim light, and decrease of fluorescence lifetime leads to reduction of photobleaching because the fluorophore spends less time in the excited state, where it is susceptible to oxygen attack. Fluorescence enhancement and reduction of photobleaching on rough metallic surfaces are usually accompanied by a loss of optical resolution due to refraction of light by particles. In the case of monolayers of silver nanoparticles, however, the surface is smooth and glossy. The fluorescence enhancement and the reduction of photobleaching are achieved without sacrificing the optical resolution of a microscope. Skeletal muscle myofibrils were used as an example, because they contain submicron structures conveniently used to define optical resolution. Small nanoparticles (diameter ~60 nm) did not cause loss of optical resolution, and they enhanced fluorescence ~500-fold and caused the appearance of a major picosecond component of lifetime decay. As a result, the sample photobleached ~20-fold more slowly than the sample on glass coverslips.

INTRODUCTION

Recently, it has become possible to study single protein molecules in a cell (1,2). The advantage of single-molecule detection (SMD) is that it studies the behavior of proteins in their native (crowded) environment, and avoids problems associated with averaging responses of an assembly of molecules with different kinetics. However, the single-molecule approach is complicated by photobleaching, which arises because the sample must be illuminated with the intense laser beam to assure an adequate signal/noise ratio.

In an earlier work, we were able to decrease photobleaching by making measurements on coverglasses coated with nanoparticles known as surface island films (SIF) (3). SIFs are nanoparticles (4–10) that can support confined charge density oscillations (11) called localized surface plasmon (LSP) polariton modes. Excitation of LSPs causes a strong enhancement of local electric field and a substantial decrease of fluorescence lifetime caused by the distance-dependent changes in the radiative decay rates (12). Enhancement of the local field allows attenuation of illumination, which leads to reduction of photodamage. At the same time, enhancement causes an effective decrease of photobleaching: although it does not change the characteristics of a fluorophore, and therefore has no effect on the intrinsic resistance to photobleaching, it increases the time that a fluorophore remains unbleached, because the sample can be illuminated with a weaker light. Decrease of fluorescence lifetime, on the other hand, leads to a decrease of the intrinsic photobleaching rate. The decrease in bleaching is mainly caused by the fact that the molecule spends less time in the excited state, where it is subject to oxygen attack. For a fluorophore in a normal nonsaturation limit (i.e., the increase in laser power causes a corresponding increase in fluorescence intensity), the decrease of fluorescence lifetime also causes an increase in quantum yield, Q. However, since the Q of rhodamine is near 1 anyway, this effect is not very significant in our experiments. For a fluorophore in a saturation limit (i.e., the increase in laser power does not cause an increase in fluorescence intensity), there is an additional effect: the decrease in fluorescence lifetime causes an increase of effective cross section for absorption, because short-lived fluorophores can now be excited, whereas long-lived ones cannot be.

As a consequence of SIF-induced field enhancement and decrease of lifetime, the rate of photobleaching of rhodamine-phalloidin-labeled actin in a myofibril placed on glass coverslips coated with SIF decreased approximately twofold in comparison with that of myofibrils placed on uncoated coverslips (3). The price of the reduction in bleaching, however, was a loss of optical resolution and loss of nonuniformity of illumination, because SIF refracted the exciting and fluorescent light, and because nanoparticles were dis-

Submitted February 4, 2008, and accepted for publication April 7, 2008.

Address reprint requests to Julian Borejdo, Dept. of Biochemistry, Health Science Center, University of North Texas, 3500 Camp Bowie Blvd., Fort Worth, TX 76107-2699. Tel.: 817-735-2106; E-mail: jborejdo@hsc.unt.edu.

Editor: Elliot L. Elson.

© 2008 by the Biophysical Society
0006-3495/08/10/3429/10 $2.00

doi: 10.1529/biophysj.108.130799

tributed randomly on the surface of a coverslip. This is a severe disadvantage of the use of SIF in SMD, because maximal optical resolution is important in resolving single molecules. Optimal resolution allows accurate definition of the region of interest (ROI) within a cell, a requirement crucial for determining a function of a specific subcellular organelle. For example, in studying the function of skeletal muscle myofibrils, it is important to place the ROI exactly at the area where actin and myosin filaments interact to produce contractile force (13). This area, known as the overlap zone, spans a distance of 0.7–0.3 μm in resting-length myofibrils (14,15), and its length is comparable to the maximal resolution of an optical microscope. The use of SIFs prevents the achievement of this resolution. In this article, we show that replacing random, multilayered SIFs with nanoparticle monolayers (NMLs) covalently bound to glass does not affect the optical resolution of the microscope, and significantly improves field enhancement and fluorescence-lifetime decrease of SIFs, thus leading to reduced photobleaching.

MATERIALS AND METHODS

Chemicals and solutions

Fluorescein-phalloidin (Fl-phalloidin), unlabeled phalloidin, phosphocreatine, creatine kinase, glucose oxidase, and catalase were from Sigma (St. Louis, MO). Rhodamine-phalloidin (Rh-phalloidin) was from Molecular Probes (Eugene, OR).

Preparation of nanoparticle monolayers

To prepare NMLs, silver colloids were prepared as previously described (16). Briefly, all necessary glassware was soaked in a base bath overnight and then washed with deionized water. A solution of 18 mg/mL silver nitrate (200 mL) was heated and stirred in a 250-mL Erlenmeyer flask at 95°C. A 0.5-mL aliquot of 34 mM trisodium citrate solution was added dropwise. The solution was stirred for 20 min and warmed to 96–98°C. Five aliquots (0.7 mL each) of 34 mM trisodium citrate were then added dropwise to the reaction mixture every 15–20 min. Stirring was continued for 25 min until the milky yellow color remained. Then, the mixture was cooled in an ice bath for 15 min. The colloids were separated by centrifugation at 3500 rpm for 6 min. The residues were collected and dissolved in 1 mM trisodium citrate. The nanoparticles were covalently attached to glass coverslips, as previously described (17). The glass coverslips were washed with Alconox soap and rinsed with distilled water. They were then soaked for 2 h in 0.1 M NaOH to activate the surface, rinsed copiously with distilled water, and soaked overnight at 80–90°C in a solution of 5% (v/v) amino-propyl-triethoxy-silane buffered with 0.1 M acetic acid (pH 5.5). Next, the coverslips were rinsed with deionized water, air dried, and placed into a petri dish for drop-coating with the solutions of small or large silver colloids. About 300 μL of the colloidal silver sols were drop-coated on the desired area of the glass coverslip. After incubation for 2 h at room temperature, the excess of colloidal silver solution was rinsed with deionized water. The glass coverslips with attached silver nanoparticles were air-dried and stored in vials.

Preparation and labeling of myofibrils

Rabbit psoas muscle was first prewashed with cold EDTA-rigor solution (50 mM KCl, 2 mM EDTA, 10 mM dithiothreitol, and 10 mM TRIS-HCl, pH 7.6) for ½ h, followed by Ca-rigor solution (50 mM KCl, 2 mM $MgCl_2$, 0.1 mM $CaCl_2$, 10 mM dithiothreitol, and 10 mM TRIS-HCl, pH 7.6). Myofibrils were made from muscle, as previously described (18). Unless otherwise indicated, myofibrils (1 mg/mL) on glass coverslips were labeled for 5 min with 0.01 μM fluorescent phalloidin + 9.99 μM unlabeled phalloidin. After labeling, myofibrils were washed by centrifugation on a desktop centrifuge at 3000 rpm for 2 min followed by resuspension in rigor solution. Myofibrillar suspension (15 μL) was placed on uncoated or coated coverslips, then covered with a glass coverslip (to avoid drying), then washed with three to four volumes of rigor solution.

Atomic force microscopy and scanning electron microscopy

Atomic force microscopic (AFM) imaging was performed on the AFM Explorer (ThermoMicroscopes/Veeco Instruments, New York) in contact scanning mode with a nonconductive silicon nitride probe (Veeco Instruments). Images were acquired at a rate of 2–5 μm/s with a resolution of 300 pixels/line. The images were processed with WSxM Ver 4.0 software for 3D analysis and with the Veeco SPMLab Ver 6.0.2 software for 2D analysis. Scanning electron microscope (SEM) images were recorded with JEOL JSM 648OLV microscope.

Measuring fluorescence spectra and bulk photobleaching

The sample was placed in the front-face configuration (45° angle with respect to the direction of the exciting beam of light) in the sample compartment of a Varian Eclipse Spectrofluorometer (Varian, San Carlos, CA). The excitation was at 475 nm. In photobleaching experiments, the observation was at 575 nm.

Measuring fluorescence lifetimes

Fluorescence lifetimes were measured by time-domain technique using FluoTime 200 fluorometer (PicoQuant, Berlin Adlershof, Germany). The sample was positioned in front-face configuration inside the fluorometer chamber. The excitation was by a 475-nm laser-pulsed diode, and the observation was through a monochromator at 575 nm with a supporting 550-nm-long wave-pass filter. The full width at half-maximum of the pulse response function was 68 ps (measured by PicoQuant). The time resolution

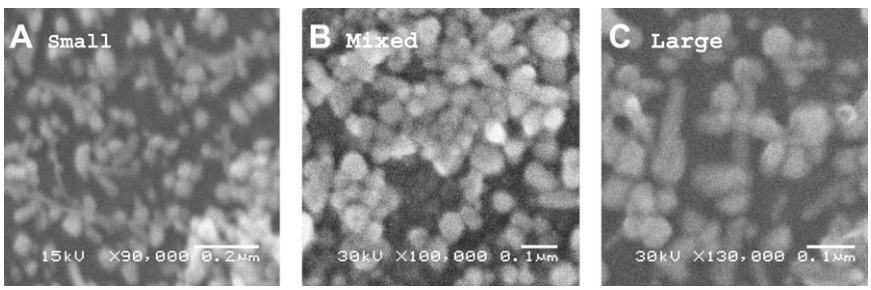

FIGURE 1 SEM images of the NML surface, with median diameters of 60, 50, and 70 nm, respectively, for small- (*A*), mixed- (*B*), and large-sized (*C*) particles.

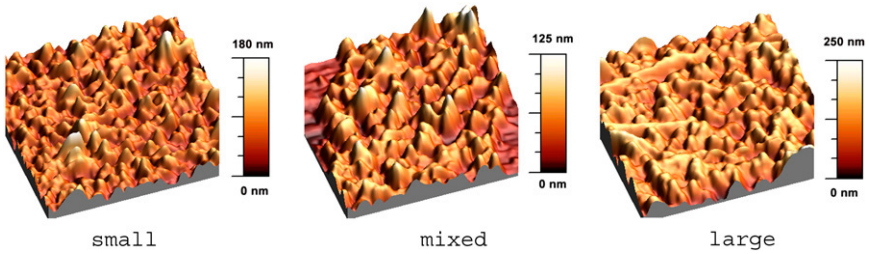

FIGURE 2 AFM images of the NML surface. All images are 2.5 × 2.5 μm.

was >10 ps. Less than 0.5% background was detected from the NML slide. The intensity decays were analyzed in terms of a multiexponential model using FluoFit software (PicoQuant).

SMD measurements

The experiments were carried out in SMD microscope described earlier (18), operating in either total internal reflection fluorescence (TIRF) or a transmitted (T) light mode. An experimental chamber was made by placing a sample on an NML-coated coverslip, sealing the sides around it with Vaseline, and covering it on top with a 24 × 24-mm glass coverslip (Fisher Scientific, Pittsburgh, PA). The chamber was placed on a moveable piezo stage (Nano-H100, Mad City Labs, Madison, WI) that was installed on the stage of an Olympus IX71 microscope. Experiments in TIRF mode were done using a commercial Olympus TIRF adaptor (Olympus, Center Valley, PA). The sample was placed NML-coated coverslip down. Experiments in T mode were done using a 1 mW beam of 543 nm light from an HeNe laser (LGP-193-249, Melles Griot, Carlsbad, CA), which entered through the back port of an Olympus IX71 microscope and was focused by the objective (Olympus PlanApo 60×, 1.45 NA) on a sample plane. The sample was placed NML-coated coverslip up. The focal spot was ~0.5 μm × −0.5 μm. This spot was made to overlap with the projection of the confocal aperture on the sample plane by adjusting the *xy* position of the focal spot with a pair of micromanipulators attached to the beam-steering post. The piezo stage was used to place the ROI in a position conjugate to the confocal aperture, as previously described (18). The same objective collected fluorescent light, which was then projected onto a tube lens. The lens focused light at the conjugate image plane. An optical fiber (whose core acted as a confocal aperture) was inserted at this plane. An avalanche photodiode (APD) (SPCM-AQR-15-FC, PerkinElmer, Wellesley, MA) collected light emerging from the aperture.

Imaging

An 60× objective with NA 1.45 was used to excite and collect the fluorescent light. Images were captured by an EMImage EM CCD camera (Hamamatsu, Japan) attached to the side port of the microscope. The pixel size of the camera was 16 × 16 μm. For the 60×, NA 1.45 objective, the back-projected size of the pixel of the camera was 267 nm and the images were undersampled by a factor of ~3.

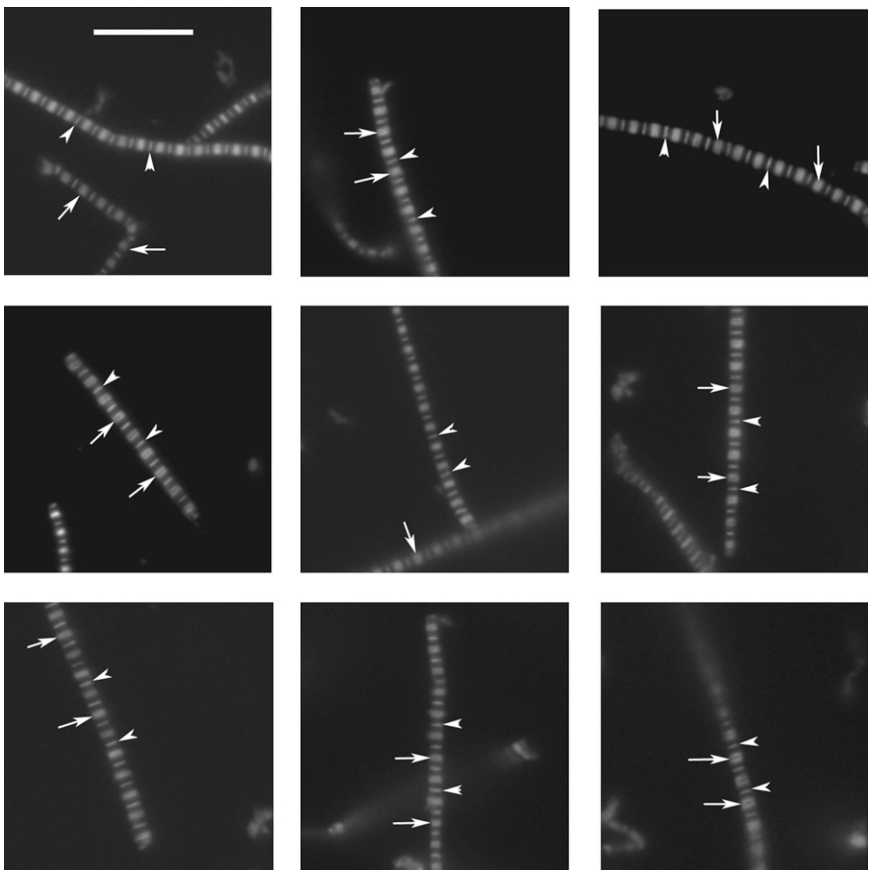

FIGURE 3 Representative images of myofibrils on glass. Arrowheads point to the Z-lines and arrows point to the H-zones. Myofibrils were labeled with 0.1 μM rhodamine phalloidin + 9.9 μM unlabeled phalloidin. Scale bar, 10 μm. TIRF excitation.

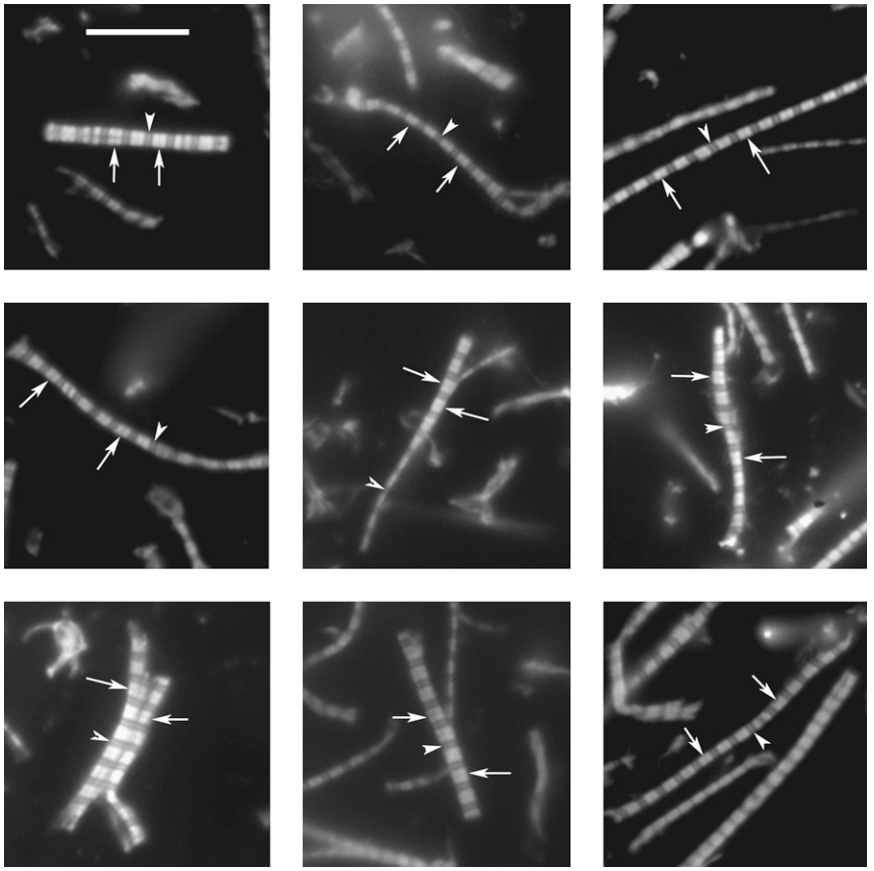

FIGURE 4 Demonstration that the quality of images is not degraded by the presence of colloid. The quality of images is as good as in the absence of colloid (Fig. 3). Arrowheads point to the Z-lines and arrows point to the H-zones. Myofibrils were labeled with 0.1 μM rhodamine phalloidin + 9.9 μM unlabeled phalloidin. Scale bar, 10 μm. TIRF excitation.

Size of the confocal aperture

The confocal aperture should be as large as possible to maximize the signal, but it makes no sense to make its projection on the sample plane smaller than the optical resolution ($\sim$0.25 μm) of the objective used here (NA 1.45). The diameter of the projection of the aperture on the object plane is equal to the diameter of the confocal aperture (D) divided by the magnification of the objective ($M = 60$), making the optimal size of the confocal aperture $D = M \times R = 15$ μm. Since there are no commercial optical fibers of this size, we used the closest available size: 8 μm single-mode fiber.

Data analysis

Data was analyzed by SigmaPlot 7 (SPSS, Chicago, IL).

RESULTS

AFM and SEM images of NML surfaces

Fig. 1 shows representative SEM images of a small-, mixed-, and large-sized NML deposited on glass. The median diameters were 60 $\pm$ 21, 50 $\pm$ 10, and 71 $\pm$ 0.20 nm (median $\pm$ SD), respectively. The average ratios of diameters in the xy plane for small, mixed, and large nanoparticles were 1.1 $\pm$ 0.2, 0.8 $\pm$ 0.08, and 1.3 $\pm$ 0.4, respectively. Fig. 2 shows representative AFM images of small, mixed and large NMLs deposited on glass. The average heights of small, mixed, and large NMLs were 40 $\pm$ 6 nm, 42 $\pm$ 9 nm, and 74 $\pm$ 10 nm (mean $\pm$ SD), respectively. The average axial ratios of small, mixed, and large NMLs were 1.5, 1.2, and 0.9, respectively. The thickness of myofibrils was estimated from AFM images by measuring the distance from the coverglass to the highest point of elevation of the O-band. In 12 measurements on phalloidin-labeled myofibrils, the average height of a myofibril was 97 $\pm$ 4 nm and the average width was 1.68 $\pm$ 0.22 μm (mean $\pm$ SEM).

Quality of images

Fig. 3 shows representative examples of myofibrils on glass. The images are of good quality, as evidenced by the fact that the Z-bands (*arrowheads*) and the H-zones (*arrows*) are well resolved. Myofibrils are particularly favorable objects for

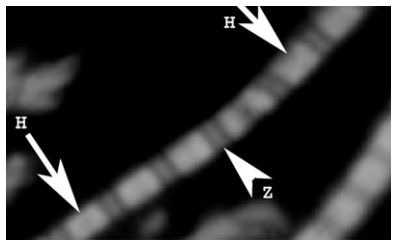

FIGURE 5 Image of myofibrils on NML, showing that the resolution is as good as on glass, as evidenced by the fact that both H-zones (*arrows*) and Z-lines (*arrowhead*) can be seen. TIRF excitation.

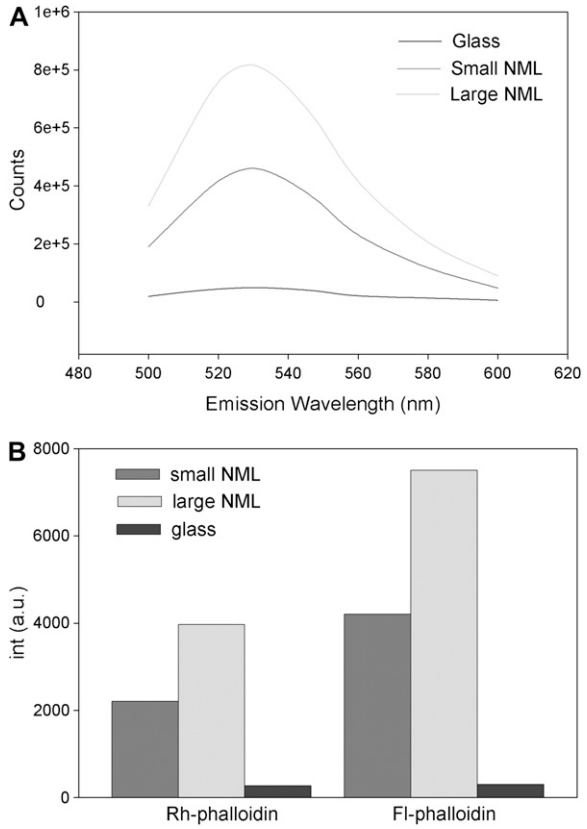

FIGURE 6 Enhancement of fluorescence by colloid monolayers. (A) Spectra of myofibrils (1 mg/mL labeled with 0.1 μM fluorescein-phalloidin) on glass coverslip coated with monoloayers containing large (*light gray*) and small (*dark gray*) colloids. Spectra were measured at a 45° angle in a Varian Eclipse spectrofluorometer. Excitation wavelength was 475 nm. The spectrum of glass alone is in black. The spectrum of colloid monolayer in the absence of muscle was comparable to glass alone. (*B*) Fluorescence intensities of myofibrils (1 mg/mL) labeled with 0.1 μM rhodamine-phalloidin (*left*) and 0.1 μM fluorescein-phalloidin (*right*). Myofibrils were on glass (*black*) coverslips or on glass coated with monoloayers containing large (*light gray*) and small (*dark gray*) colloids. The intensities were measured at an orthogonal excitation, at 560 nm (*left*) and 530 nm (*right*) in a Varian Eclipse spectrofluorometer. Excitation wavelength was 475 nm.

testing optical resolution, because the widths of Z-lines and H-zones are ~0.25 μm, approximately equal to the optical resolution of the NA 1.45 objective using green light. Fig. 4 shows representative examples of myofibrils on mixed NMLs. Fig. 5 (magnification of Fig. 4, *lower right*) shows that the resolution of the Z-bands (*arrowheads*) and the H-zones (*arrows*) is as good as that for myofibrils on glass. The intensity is larger in Fig. 4 than in Fig. 3, consistent with the fact that colloids increase brightness (see below).

Increase of brightness

Bulk measurements

The diameter of the excitation beam was ~1 mm and the thickness of the sample was ~100 nm (see above), giving a detection volume of $\sim 10^{-10}$ L. For myofibrils labeled with 0.1 μM fluorescent phalloidin + 9.9 μM nonfluorescent phalloidin, this means we observed $\sim 10^6$–10^7 molecules of the dye. Fig. 6 *A* compares emission spectra of myofibrils on glass coverslips coated with NML with spectra of myofibrils on plain glass. No differences in the emission spectra were detected. Fig. 6 *B* compares peak intensities of myofibrils labeled with Rh- (*left*) or Fl-phalloidin (*right*). The peak fluorescence intensity of Rh-phalloidin-labeled myofibrils on small- and large-NML-coated coverslips was enhanced ~7 and 13 times, respectively, compared with that on plain glass coverslips. The peak fluorescence intensity of Fl-phalloidin-labeled myofibrils on small- and large-NML-coated coverslips was, respectively, 18 and 33 times that on plain glass coverslips (Table 1).

SMD measurements

Because the myofibril is <100 nm thick, it makes no difference as far as the number of excited molecules are concerned, whether SMD experiments are carried out using transmitted or TIRF illumination. The signal from a myofibril was measured by positioning the O-band over the projection of the confocal aperture on the sample plane, as described in Borejdo et al. (19). The focused laser spot was previously positioned over this projection. The detection volume is $\pi \times (D/2)^2 \times H$, where H is the average thickness of a myofibril. The average thickness was ~100 nm (see above). The detection volume was $\sim 20 \times 10^{-18}$ L. Actin concentration in muscle (0.6 mM) implies that there were ~7200 actin protomers in this volume. The ratio of fluorescent phalloidin to nonfluorescent phalloidin was fixed at 1:1000, suggesting that the signal was contributed by, on average, seven to eight actin molecules. In five experiments, enhancements were 84 ± 18 and 540 ± 81 for mixed and small colloids, respectively (Table 1).

Decrease of fluorescence lifetime

Bulk measurements

Myofibrils were labeled with fluorescein-phalloidin (rhodamine experiments are impossible–there are no green pulsed laser diodes yet).

Glass. The decay of fluorescence of myofibrils on glass (Fig. 7 *A*) was best fitted by two exponentials with lifetimes

TABLE 1 Effect of NML on enhancement of fluorescence

		Intensity (fold over glass)	
		Rhodamine	Fluorescein
Bulk	Glass	1	1
	Mixed	–	–
	Small	7	18
	Large	13	33
SMD	Glass	1	–
	Mixed	84 ± 18	–
	Small	540 ± 81	–

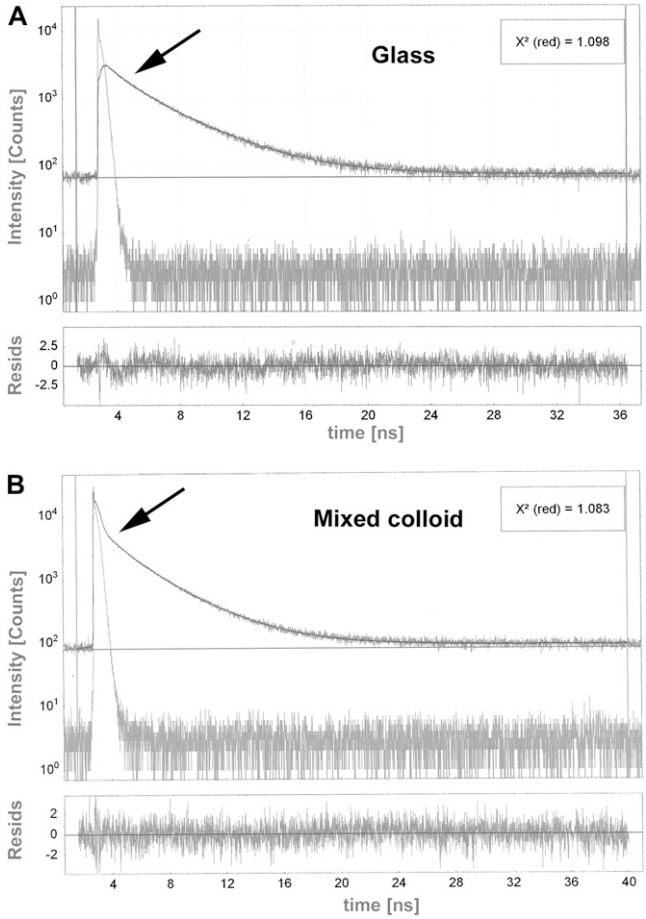

FIGURE 7 Decrease of fluorescence lifetime by mixed-size NML. (*A*) Lifetime signal from myofibrils on glass (*blue*). The signal is best fitted (*black line*) by the two exponentials with lifetimes $\tau_1 = 3.596$ and $\tau_2 = 1.138$ ns, with relative contributions to the total amplitude of 55.3% and 44.7%, respectively. The gray signal is the exciting pulse from the diode laser. The bottom panel shows the residual fit to all 8767 data points. (*B*) Lifetime signal from myofibrils on glass coated with a mixed-size SIF monolayer (*black*) is best fitted (*black line*) by three exponentials with lifetimes $\tau_1 = 3.396$ ns, $\tau_2 = 0.1.420$ ns, and $\tau_3 = 0.146$ ns, with relative contributions to the total amplitude of 13.5%, 16.3%, and 70.2%, respectively. The arrows point to the fast decay of fluorescence. The gray signal is the exciting pulse. The bottom panel shows the residual fit to all 9604 data points. The 1-mg/mL myofibrils were labeled with 0.1 μM fluorescein-phalloidin.

$\tau_1 = 3.596$ and $\tau_2 = 1.138$ ns with the relative contributions to the total amplitude of 55.3% and 44.7%, respectively. The amplitude weighted average lifetime was 2.498 ns.

Mixed NML. The decay on mixed NML was considerably different (Fig. 7 *B*). The decay of fluorescein was now best fitted by three exponentials with lifetimes $\tau_1 = 3.396$ ns, $\tau_2 = 1.420$ ns, and $\tau_3 = 0.146$ ns, with relative contributions to the total amplitude of 13.5%, 16.3%, and 70.2%, respectively. The amplitude-weighted average lifetime decreased to 0.791 ns. Thus, the application of NML caused the appearance of an ultrashort component contributing >70% to the signal amplitude, and caused the amplitude-weighted average lifetime to decrease more than threefold.

Small NML. Fig. 8 *A* shows that the addition of small NML caused the fluorescence lifetime to decrease. The lifetime signal from myofibrils on small NML was best fitted by three exponentials with lifetimes $\tau_1 = 3.448$ ns, $\tau_2 = 1.225$ ns, and $\tau_3 = 0.168$ ns, with relative contributions of 18.5%, 21.5%, and 60.0%, respectively, to the total amplitude. The amplitude-weighted average lifetime was 1.006 ns. Thus, the application of small NML caused the appearance of an ultrashort component contributing >60% to the signal ampli-

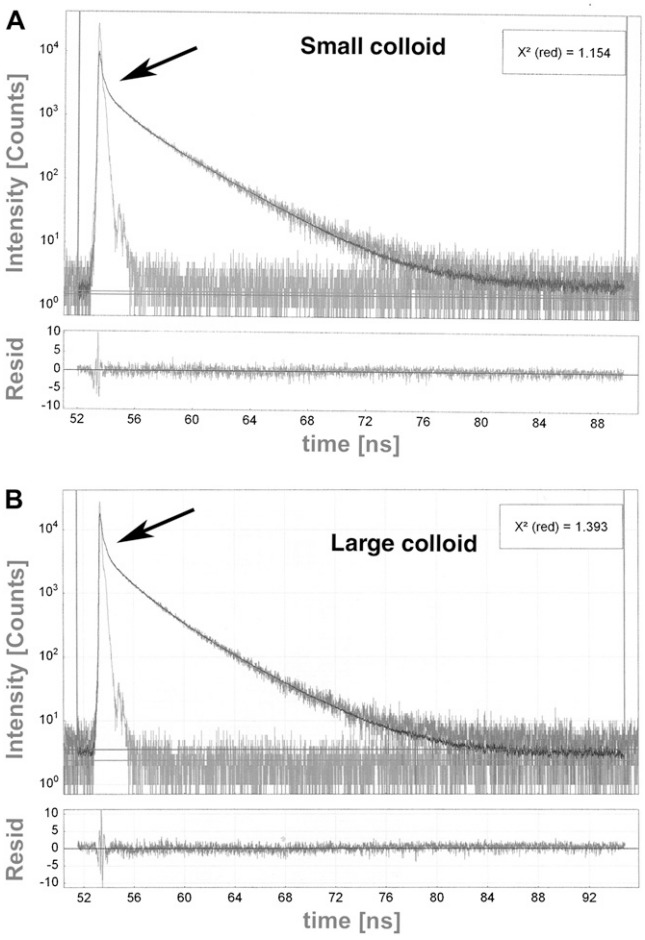

FIGURE 8 Decrease of fluorescence lifetime by small and large NML. (*A*) Lifetime signal from myofibrils on the small NML (*black*). The signal is best fitted (*black line*) by three exponentials with lifetimes $\tau_1 = 3.448$ ns, $\tau_2 = 1.225$ ns, and $\tau_3 = 0.168$ ns, with relative contributions to the total amplitude of 18.5%, 21.5%, and 60.0%, respectively. The gray signal is the exciting pulse from the diode laser. The bottom panel shows the residual fit to all 9445 data points. The arrow points to the fast decay of fluorescence. (*B*) Lifetime signal from myofibrils on the large NML (*black*). It is best fitted (*black line*) by four exponentials with lifetimes $\tau_1 = 1.787$ ns, $\tau_2 = 0.256$ ns, $\tau_3 = 3.983$ ns, and $\tau_4 = 0.014$ ns, with relative contributions to the total amplitude of 0.8%, 1.7%, 0.4%, and 97.1%, respectively. The arrow points to the fast decay of fluorescence. The gray signal is the exciting pulse. The bottom panel shows the residual fit to all 10828 data points. Myofibrils labeled with 0.1 μM fluorescein-phalloidin + 9.9 μM unlabeled phalloidin. TIRF illumination was used on 1-mg/mL myofibrils labeled with 0.1 μM fluorescein-phalloidin.

TABLE 2 Effect of NML on lifetime

		Lifetime (ns)	SD	% Contribution
Bulk	Glass	3.596	0.038	55.3
		1.138	0.050	44.7
	Mixed	3.396	0.024	13.5
		1.420	0.028	16.3
		0.146	0.005	70.2
	Small	3.448	0.095	18.5
		1.225	0.061	21.5
		0.168	0.020	60.0
	Large	3.983	0.063	0.4
		1.787	0.018	0.8
		0.256	0.013	1.7
		0.014	0.002	97.1

Standard deviations from 67% confidence intervals were determined by FluoFit4 (PicoQuant). Relative contributions to the overall intensity are given in column 3.

tude, and caused amplitude-weighted average lifetime to decrease more than twofold.

Large NML. Addition of large NML (Fig. 8 *B*) augmented the fast decay of fluorescein-labeled myofibrils even more (*arrow*). The decay was best fit now by four exponentials with lifetimes $\tau_1 = 3.983$ ns, $\tau_2 = 1.787$ ns, $\tau_3 = 0.256$ ns, and $\tau_4 = 0.014$ ns, with relative contributions of 0.4%, 0.8%, 1.7%, and 97.1%, respectively, to the total amplitude. The amplitude-weighted average lifetime decreased to 0.048 ns. The application of large NML caused the appearance of an ultrashort component contributing >97% to the signal amplitude, and caused the amplitude-weighted average lifetime to decrease >48-fold. Lifetime data is summarized in Table 2.

To fit the data accurately in the presence of the monolayer of silver nanoparticles, it was necessary to use a more complex decay model (three exponents for mixed and small NMLs and four exponents for large NMLs). In these decays,

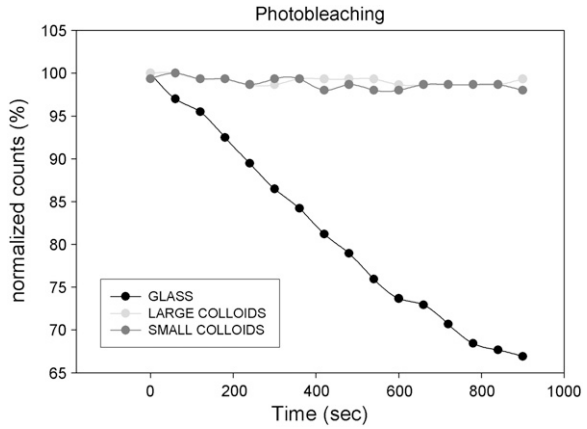

FIGURE 9 Photobleaching of myofibrils in the bulk solution. The sample was positioned in front-face configuration inside the fluorometer chamber. Λ_{exc} was 475 nm and λ_{em} 575 nm. Time 0 is after exposing the sample to light for 10 s. Consecutive readings were taken every 60 s, for a total of 1000 s. The 1-mg/mL myofibrils were labeled with 0.1 μM fluorescein-phalloidin.

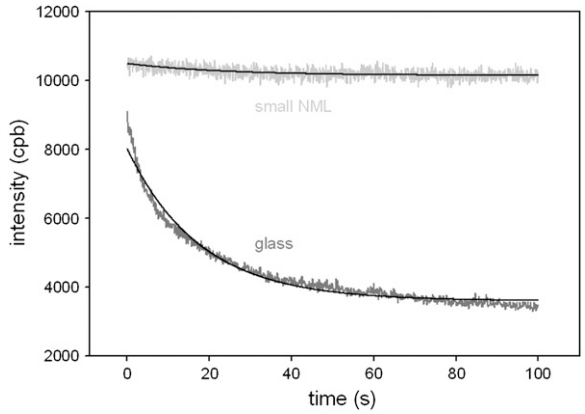

FIGURE 10 Comparison of the rates of photobleaching of the myofibrillar overlap zone on small NML. Myofibrils (1 mg/mL) were labeled with 0.01 μM rhodamine-phalloidin + 9.99 μM unlabeled phalloidin. The overlap zone of a myofibril was viewed by SMD microscopy through an 8-μm confocal aperture. The three-parameter single-exponential fits for glass and NML are shown in black. The objective NA = 1.45. cpb are counts/100-ms bin. TIRF excitation.

the contributions of short-lived components were very high, the biggest being for large NML (97%). It is often a difficult task to resolve such short components, especially when their contribution to the total decay is weak. However, in the case of a very high contribution, the resolution is much more reliable, as can be seen in Table 2 (*SD column*).

SMD measurements

Lifetimes were only measured in the bulk. We do not yet have the ability to measure lifetimes with a microscope.

Decrease of photobleaching

As in the case of the increase of brightness, the decrease of photobleaching was different in bulk and SMD measurements.

Bulk measurements

Fig. 9 shows the decay of fluorescence in a bulk sample. The sample was positioned in front-face configuration inside the

TABLE 3 Effect of NML on half-times of bleaching

		Half-time of bleaching (s)
Bulk	Glass	300
	Mixed	–
	Small	At least 2000
	Large	At least 2000
SMD	Glass	11 ± 4
	Mixed	56 ± 22
	Small	At least 200
	Large	69 ± 25

Bulk measurements were done on 1 mg/mL myofibrils labeled with 10 nM fluorescein-phalloidin + 10 μM unlabeled phalloidin. SMD measurements were done on 1 mg/mL myofibrils labeled with 10 nM rhodamine-phalloidin + 10 μM unlabeled phalloidin.

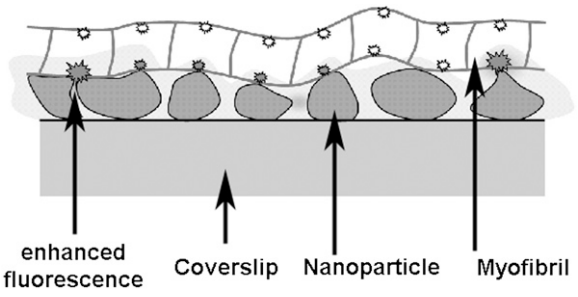

FIGURE 11 Schematic diagram of a myofibril on a glass coverslip with NML-coated surface.

fluorometer chamber. Excitation was at 475 nm and observation was through a monochromator at 575 nm. Time 0 was after exposing the sample to the laser light for 10 s. Consecutive readings were taken every 60 s for a total of 1000 s. The half-time of photobleaching for the sample on glass was ~300 s, and that for the sample on small and large NMLs was ≥2000 s.

SMD measurements

Fig. 10 compares the rate of photobleaching of the myofibrillar overlap zone on glass and on coverslips coated with NML. Small NML is shown as an example. The signal from the myofibril (*light gray*) was enhanced 90-fold compared with the signal on glass (*gray*). The average halftime of decay was at least 200 s. We were unable to determine exactly the rate of photobleaching, because it depended critically on the choice of baseline: the lower the baseline, the slower the decay. For example, if the baseline in Fig. 10 was chosen to be 10,000, the rate for NML was approximately equal to the rate for glass. The average halftimes for mixed and large colloids were 56 ± 22 s and 69 ± 25 s (Table 3).

DISCUSSION

The large enhancement of the excitation field made possible illumination with a weaker laser beam, which leads to a reduction of photodamage. The interactions between the LSPs and the fluorophores led to a significant increase of the spontaneous radiative rate of a fluorophore (20). Such enhancement is well known in surface plasmon resonance signals (21). The intensity enhancement around a spheroid is calculated analytically below assuming the Rayleigh limit. We also make accurate calculations (not assuming the Rayleigh limit) by the use of vector prolate spheroidal functions (22). Fig. 11 schematically illustrates the experimental arrangement. Nanoparticles and myofibrils are deposited on a glass coverslip. The Z-dimension of nanoparticles is comparable to the size of the myofibrils (23). We assume that nanoparticles are spheroid. The equation to be solved is

$$\nabla^2 V = 0,$$

where V and $\varepsilon(\partial V/\partial\alpha)$ are continuous at the spheroidal surface and $V \rightarrow Ez$ at infinity. E is the magnitude of the applied electric field and ε is the permittivity. Prolate spheroidal coordinates (α, β, ϕ) are used:

$$\begin{cases} x = f\sinh(\alpha)\sin(\beta)\cos(\varphi) \\ y = f\sinh(\alpha)\sin(\beta)\sin(\varphi) \\ z = f\cosh(\alpha)\cos(\beta)\cos(\varphi) \end{cases}.$$

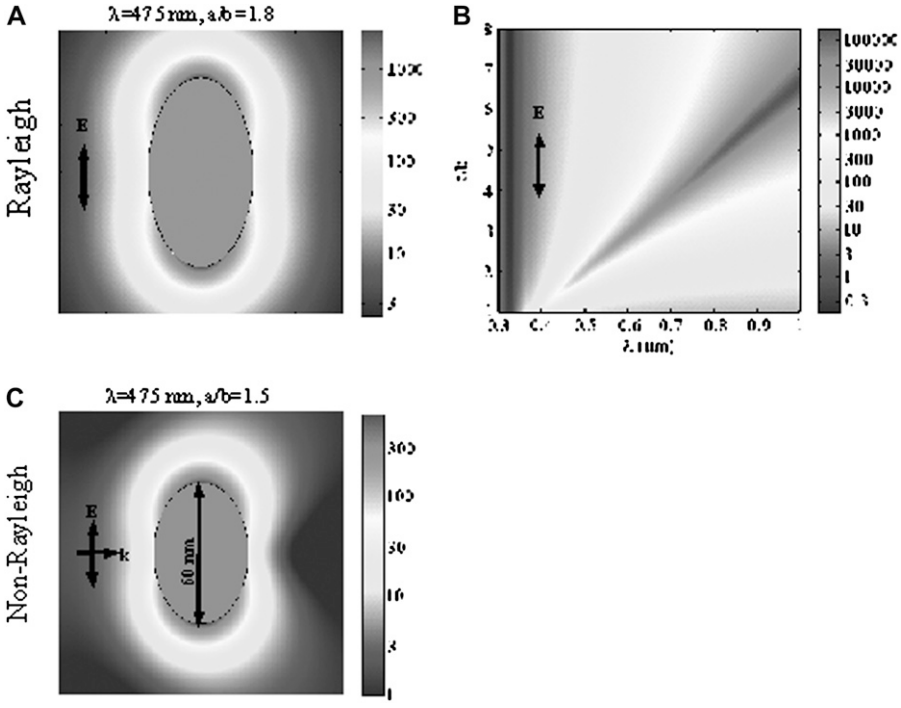

FIGURE 12 Intensity enhancement of silver spheroid particles in water. (*A*) The intensity enhancement is in the Rayleigh limit, i.e., the particles are small compared to the wavelength. (*B*) The intensity enhancement at a spheroidal tip versus wavelength and axial ratio. (*C*) The intensity enhancement around a spheroid. The Rayleigh limit is not assumed. The calculations are exact using spheroidal wave functions.

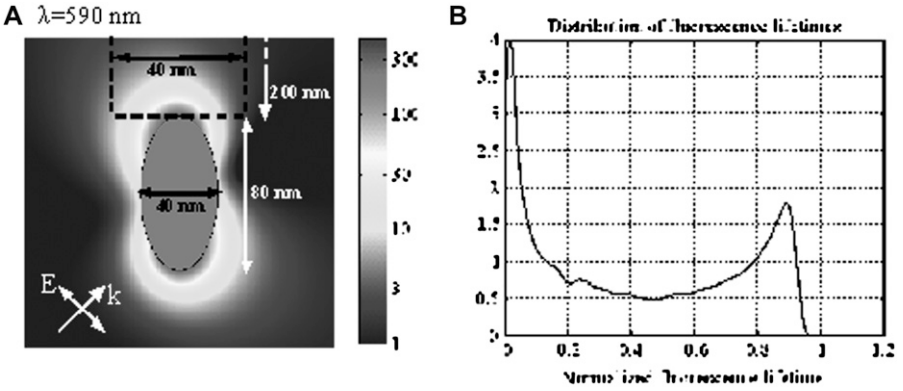

FIGURE 13 Calculations to mimic the experimental setup, showing (*A*) the intensity enhancement, and (*B*) the distribution of lifetimes of fluorophores within the box.

f is a parameter regulating the size of the spheroid, and the spheroidal surface is determined by the equation $\alpha = \alpha_0$ for some constant α_0.

Solving the differential equation gives the analytic solution

$$V = Ef(\cosh(\alpha) + AQ_1(\cosh(\alpha)))\cos(\beta)$$

$$A = \frac{(\varepsilon_i - \varepsilon_o)\cosh(\alpha_0)}{\varepsilon_i \cosh(\alpha_0)Q_1'(\cosh(\alpha_0)) - \varepsilon_o Q_1(\cosh(\alpha_0))}.$$

ε_i is the permittivity inside the spheroid (in this case, silver, and it is complex), and ε_o is the permittivity outside (in this case, water, with a value of 1.33^2). Q_1 is a Legendre function of the second kind, and Q_1' is its derivative. Q_1 is given by

$$Q_1(u) = \frac{u}{2}\ln\left(\frac{u+1}{u-1}\right) - 1.$$

Fig. 12 shows the results of calculations of intensity enhancement of silver spheroids in water: the enhancement depends sharply on the values of axial ratio (a/b) and wavelength (λ). In general, the enhancement increases with a/b and decreases with λ. Fig. 12 *B* shows that for $\lambda = 530$ nm and $a/b = 1.5$, the enhancement is ~1000, in good agreement with the experiment (540-fold, Table 1). The fact that the enhancement was smallest for mixed particles (Table 1, *SMD*) is consistent with the theory, because large nanoparticles were the most symmetrical. Fig. 12 *A* shows that 1000-fold enhancement stretches at least to 10 nm beyond the limit of the nanoparticles, which is consistent with the idea that fluorophores nearest to the surface contribute the most to the enhancement (Fig. 11). The fact that enhancement in the bulk is smaller than in SMD may be due to the fact that the incident angle of the exciting wave is different in each case.

In the non-Rayleigh limit procedure, a series of vector spheroidal wave functions is used that is in principle similar to the Mie series for spheres, but more complicated. This case is described in Calander and Willander (22).

To calculate the influence of nanoparticles on the bulk fluorescence lifetime, we assume that the lifetime of a fluorophore is inversely proportional to the electromagnetic intensity enhancement, due to the reciprocity of energy flow. The intensity enhancement is calculated (by spheroidal wave functions) at a couple of thousand points equally distributed within a box at the spheroid surface ($40 \times 40 \times 200$ nm, Fig. 13 *A*). The enhancements at these points are used to calculate the distribution of lifetimes of fluorophores within the box (Fig. 13 *B*). It can be seen that, in agreement with experiment, the short lifetime is now the most prominent. The overall combined fluorescence intensity enhancement is 2.6 (assuming the same enhancement for emission and excitation), consistent with a small intensity enhancement observed in bulk (Table 1). At very strong field enhancements, one may speculate that resonance fluorescence may occur, making emission and excitation combine to give higher fluorescence intensity enhancement (up to a limit of 94.9 in this case). The

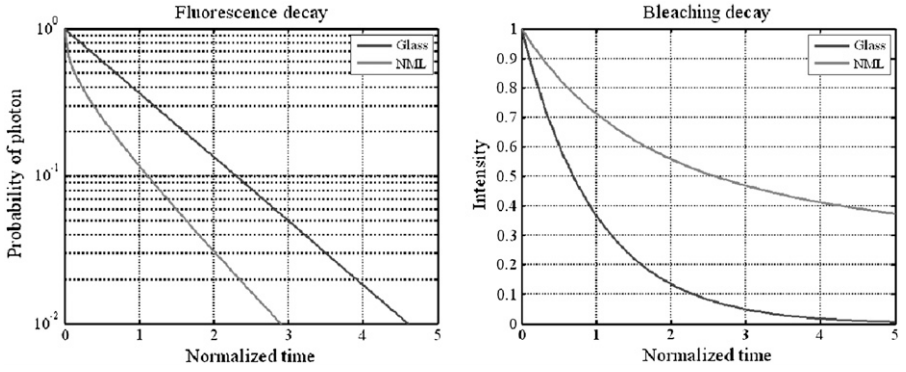

FIGURE 14 The calculation of fluorescence (*left*) and bleaching (*right*) lifetimes using spheroidal wave functions at a couple of thousand points equally distributed within a box defined in Fig. 13.

very high enhancement found experimentally in some cases may be due to this. One may also speculate that dipole-dipole interactions between the LSPs further increase the enhancement (24).

Fig. 14 shows the calculations of fluorescence (*left*) and bleaching (*right*) lifetimes using the above-described methods. The bleaching is inversely proportional to the time spent in the excited state, i.e., the fluorescence lifetime. Fig. 14 *left* clearly shows the appearance of a short lifetime component due to the increase in radiative rate. Experimentally, the effect was most dramatic when the relative contributions of the slow- and fast-decay components of fluorescence intensity were considered. There was no picosecond decay on glass, whereas on mixed, small, and large NML, such decay constituted ~70%, 60%, and 97%, respectively, of the amplitude.

Preservation of the optical resolution is important in SMD, because it allows accurate definition of the ROI within a cell. In the example used here, skeletal muscle myofibrils, it is important to place the ROI exactly at the area where myosin cross-bridges interact with actin. This interaction occurs within the area where cross-bridges of thick, myosin-containing filaments overlap with thin, actin-containing filaments. The area spans the distance, which depends on the resting length of the muscle but is typically of the order of the optical resolution of the microscope (14,15). Application of silver island films in a previous study (3) did not preserve resolution because of light refraction by multiple layers of silver nanoparticles.

It is important to point out that reduction of photobleaching by NML occurred on plain glass. This is in contrast to our earlier finding, that reduction became significant only when myofibrils were placed on a high-refractive-index surface (3). However, high-refractive-index (sapphire-based) coverslips are expensive (they cannot be reused after coating with NML) and require the use of rapidly drying and toxic immersion oil with a high index of refraction (1.78).

We thank Ewa Goldys for SEM measurements. This publication was made possible by grant RO1 AR048622 from the National Institutes of Health and by a Texas Emerging Technology Fund grant to the University of North Texas Health Science Center's Center for Commercialization of Fluorescence Technologies.

REFERENCES

1. Betzig, E., R. J. Chichester, F. Lanni, and D. L. Taylor. 1993. Near field fluorescence imaging of cytoskeletal actin. *Bioimaging.* 1:129–133.
2. Betzig, E., G. H. Patterson, R. Sougrat, O. W. Lindwasser, S. Olenych, J. S. Bonifacino, M. W. Davidson, J. Lippincott-Schwartz, and H. F. Hess. 2006. Imaging intracellular fluorescent proteins at nanometer resolution. *Science.* 313:1642–1645 Epub 2006 Aug 10.
3. Muthu, P., I. Gryczynski, Z. Gryczynski, J. Talent, I. Akopova, K. Jain, and J. Borejdo. 2007. Decreasing photobleaching by silver island films: application to muscle. *Anal. Biochem.* 366:228–236.
4. Weitz, D. A., S. Garoff, C. D. Anson, and T. J. Gramila. 1982. Fluorescent lifetimes of molecules on silver-island films. *Opt. Lett.* 7: 89–91.
5. Leitner, A., M. E. Lippitch, S. Draxler, M. Riegler, and F. R. Aussenegg. 1985. Fluorescence properties of dyes absorbed to silver islands, investigated by picosecond techniques. *Appl. Phys. B.* 36:105–109.
6. Gryczynski, I., J. Malicka, Y. Shen, Z. Gryczynski, and J. R. Lakowicz. 2002. Multiphoton excitation of fluorescence near metallic particles: enhanced and localized excitation. *J. Phys. Chem. B.* 106: 2191–2195.
7. Maliwal, B. P., J. Malicka, I. Gryczynski, Z. Gryczynski, and J. R. Lakowicz. 2003. Fluorescence properties of labeled proteins near silver colloid surfaces. *Biopolymers.* 70:585–594.
8. Geddes, C. D., H. Cao, I. Gryczynski, Z. Gryczynski, and J. R. Lakowicz. 2003. Metal-enhanced fluorescence (MEF) due to silver colloid on a planar surface: Potential applications of indocyanine green to in vivo imaging. *J. Phys. Chem. A.* 107:3443–3449.
9. Malicka, J., I. Gryczynski, and J. R. Lakowicz. 2003. DNA hybridization assays using metal-enhanced fluorescence. *Biochem. Biophys. Res. Commun.* 306:213–218.
10. Malicka, J., I. Gryczynski, J. Fang, and J. R. Lakowicz. 2002. Photostability of Cy3 and Cy5-labeled DNA in the presence of metallic silver particles. *J. Fluoresc.* 12:439–447.
11. Hayashi, S. 2001. Spectroscopy of gap modes in metal particle-surface systems. *In* Topics in Applied Physics, Near Field Optics and Surface Plasmon Polaritons, Vol. 81. S. Kawata, editor. Springer-Verlag, New York. 71–95.
12. Lakowicz, J. R., Y. Shen, S. D'Auria, J. Malicka, J. Fang, Z. Gryczynski, and I. Gryczynski. 2002. Radiative decay engineering. 2. Effects of silver island films on fluorescence intensity, lifetimes, and resonance energy transfer. *Anal. Biochem.* 301:261–277.
13. Borejdo, J., J. Talent, I. Akopova, and T. P. Burghardt. 2006. Rotations of a few cross-bridges in muscle by confocal total internal reflection microscopy. *Biochim. Biophys. Acta.* 1763:137–140.
14. Gordon, A. M., A. F. Huxley, and F. J. Julian. 1966. The variation in isometric tension with sarcomere length in vertebrate muscle fibres. *J. Physiol.* 184:170–192.
15. Gordon, A. M., A. F. Huxley, and F. J. Julian. 1966. Tension development in highly stretched vertebrate muscle fibres. *J. Physiol.* 184:143–169.
16. Lukomska, J., I. Gryczynski, J. Malicka, S. Makowiec, J. R. Lakowicz, and Z. Gryczynski. 2006. One- and two-photon induced fluorescence of Pacific blue-labeled human serum albumin deposited on different core size silver colloids. *Biopolymers.* 81:249–255.
17. Keating, C. D., M. D. Musick, M. H. Keefe, and M. J. Natan. 1999. Kinetics and thermodynamics of Au colloid monolayer self-assembly. *J. Chem. Educ.* 76:949–955.
18. Borejdo, J., Z. Gryczynski, N. Calander, P. Muthu, and I. Gryczynski. 2006. Application of surface plasmon coupled emission to study of muscle. *Biophys. J.* 91:2626–2635.
19. Borejdo, J., P. Muthu, J. Talent, I. Akopova, and T.P. Burghardt. 2007. Rotation of actin monomers during isometric contraction of skeletal muscle. *J. Biomed. Opt.* 12:014013.
20. Lakowicz, J. R., J. Malicka, I. Gryczynski, Z. Gryczynski, and C. D. Geddes. 2003. Radiative decay engineering: the role of photonic mode density in biotechnology. *J. Phys. D. App. Physics.* 36:R240–R249.
21. Natan, M. J., and A. L. Lyon. 2002. Surface plasmon resonance biosensing with colloidal Au amplification. *In* Metal Nanoparticles. D. L. Feldheim and C. A. Foss, editors. New York: Marcel Dekker. 183–205.
22. Calander, N., and M. Willander. 2002. Theory of surface-plasmon resonance optical-field enhancement at prolate spheroids. *J. Appl. Phys.* 92:4878–4884.
23. Muthu, P., I. Gryczynski, Z. Gryczynski, J. M. Talent, I. Akopova, and J. Borejdo. 2008. Decreasing photobleaching by silver nanoparticles on metal surfaces: application to muscle myofibrils. *J. Biomed. Opt.* In press.
24. Barnett, A., E. Matveeva, I. Gryczynski, Z. Gryczynski, and E. Goldys. 2007. Coupled plasmon effects for the enhancement of fluorescent immunoassays. *Physica B (Amsterdam).* 394:297–300.